Inorganic Chemistry

Article

pubs.acs.org/IC

$Ln(IO_3)_3$ (Ln = Ce, Nd, Eu, Gd, Er, Yb) Polycrystals As Novel Photocatalysts for Efficient Decontamination under Ultraviolet Light Irradiation

Wenjun Wang,[†] Hefeng Cheng,[†] Baibiao Huang,*[,†] Xinru Li,[‡] Xiaoyan Qin,[†] Xiaoyang Zhang,[†] and Ying Dai[‡]

[†]State Key Laboratory of Crystal Materials, Shandong University, Jinan 250100 (P. R. China)

[‡]School of Physics, Shandong University, Jinan 250100 (P. R. China)

Supporting Information

ABSTRACT: $Ln(IO_3)_3$ (Ln = Ce, Nd, Eu, Gd, Er, Yb) polycrystals were hydrothermally synthesized using lanthanide nitrate or lanthanide oxide and iodic acid as precursors. X-ray diffraction was used to characterize the crystal structures of the $Ln(IO_3)_3$ products. Scanning electron microscopy was carried out to observe the microscopic morphologies. The lattice spacings were studied by high-resolution transmission electron microscopy and selected area electron diffraction. We evaluated the photocatalytic efficiency by decomposing methyl orange dye under ultraviolet light irradiation, and the $Ln(IO_3)_3$ products show excellent photocatalytic properties. To rule out the effect of photosensitization, 2,4-dichlorophenol was also photodegraded. As one of the key factors of photocatalysis, ultraviolet−visible diffuse reflectance spectra of the $Ln(IO_3)_3$ samples were also studied, and all products have strong absorption in the ultraviolet region.

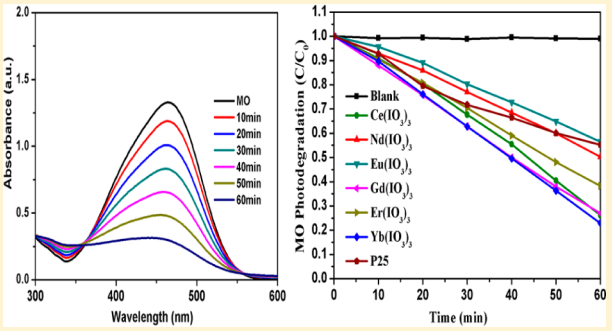

INTRODUCTION

In the periodic table, from element 57 (La) to element 71 (Lu), there are 15 kinds of elements composed of lanthanide (Ln) elements, also known as rare-earth elements, together with Sc and Y. The content of Ln elements in the earth's crust reaches 0.01534, so the rare-earth element is not rare in fact. China is rich in Ln reserves, and leads the world in this regard. The outmost two electronic shells of Ln elements are similar, and the inner 4f electronic shells are different. The outmost electrons can shield inner electrons, so the 4f electrons have a very minimal impact on the chemical properties of Ln compounds. Therefore, the structural, electronic, and energetic properties of Ln elements are similar, and these metals display a predominantly trivalent chemistry.[1] Ln-based compounds have been found to exhibit good efficiency in fields such as luminescence,[2−6] proton-conductivity,[7,8] catalysis,[9−11] and gas storage.[12,13]

Recently, Ln elements have been widely used in photocatalytic applications[14−16] as doping ions in traditional photocatalytic materials like TiO_2,[17,18] BiOCl,[19] CdS,[20] etc. In these photocatalytic systems, Ln elements act as upconverter that sum the energies of near-infrared (NIR) quanta to emit a quantum of higher energy. For instance, in Qin's study,[17] the YF_3:Yb^{3+}, Tm^{3+}/TiO_2 core/shell nanoparticles absorb NIR light and emit ultraviolet (UV) light, and TiO_2 is excited to generate holes and electrons by UV light. Li et al.[19] synthesized BiOCl:Er^{3+}/Yb^{3+} polycrystallines in which UV, violet, green, red, and NIR upconversion emissions have been observed from Er^{3+} ion under the 980 nm excitation. Nevertheless, the photocatalytic properties are very poor, and the efficiencies are very low. Importantly, Ln compounds can also absorb UV light, but the photocatalytic properties under UV light still remains unexplored. Lately, our group has first employed $BiOIO_3$ to dye photodegradation and reported its excellent photocatalytic property.[21] Iodates have become a kind of promising photocatalyst and have a promising application. Ln elements, which are used as luminescent materials, are diversiform and abundant in the earth. It is very meaningful to study the properties of Ln elements and make Ln materials widely used in various domains. We followed our previous research about $BiOIO_3$ to study the photocatalytic properties of Ln iodate materials to extend Ln elements' potential usage. To our knowledge, there have been no reports on directly utilizing Ln iodate compounds as photocatalytic materials.

We hypothesize that Ln compounds can be used in photocatalysis. In this study, some $Ln(IO_3)_3$ compounds (Ln = Ce, Nd, Eu, Gd, Er, Yb) were hydrothermally synthesized and studied for their photocatalytic properties. $Ln(NO_3)_3$ or Ln_2O_3 and HIO_3, which are environmentally friendly, were used as the sources of Ln and IO_3, respectively. UV−vis (vis = visible) diffuse reflectance spectra (DRS) of the $Ln(IO_3)_3$ samples were

Received: January 6, 2014
Published: May 5, 2014

   dx.doi.org/10.1021/ic500027f | Inorg. Chem. 2014, 53, 4989−4993

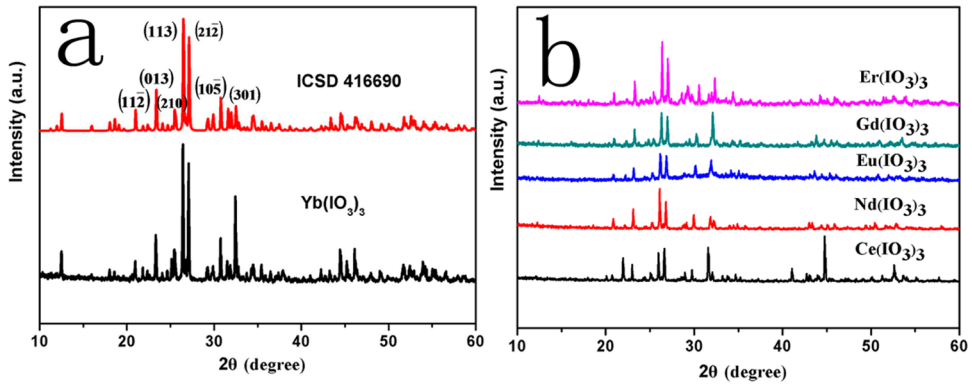

Figure 1. XRD patterns of as-prepared and standard $Yb(IO_3)_3$ (a), and other $Ln(IO_3)_3$ products (b).

studied, and all products have strong absorption in the UV region. We evaluated the photocatalytic efficiency by decomposing methyl orange (MO) dye under UV irradiation. To exclude the effect of photosensitization, 2,4-dichlorophenol (2,4-DCP) was also photodegraded.

EXPERIMENTAL SECTION

Preparation. The chemicals were analytic reagents without being purified. In a typical process, 2 mmol of lanthanide nitrate $Ln(NO_3)_3$ or 1 mmol of lanthanide oxide Ln_2O_3 (Ln = Ce, Nd, Eu, Gd, Er, Yb) was put into 80 mL of distilled water under magnetic agitation. After that, 6 mmol (1.056 g) of iodic acid was mixed with the aforesaid suspension. The mixture was stirred for 1 h to disperse uniformly and transferred to a 100 mL Teflon-lined stainless-steel autoclave. Afterward, the reactor was treated and maintained at 230 °C for 24 h, and then it was cooled to room temperature naturally. The final sample was collected, washed several times with distilled water, and dried in a desiccator overnight.

Characterization. X-ray powder diffraction (XRD) patterns were recorded on a X-ray diffractometer (Bruker AXS D8) using Cu Kα radiation (λ = 1.5418 Å) with 2θ from 10 to 60°. High-resolution transmission electron microscopy (HRTEM) and selected area electron diffraction (SAED) were performed by JEOL JEM-2100F (200 kV). The morphologies of the products were observed by scanning electron microscopy (SEM) on a Hitachi S-4800 microscope. UV−vis DRS spectra were obtained on a UV−vis spectrophotometer (Shimadzu UV 2550) over the range of 200−800 nm, and $BaSO_4$ was used as a reference.

Electronic Band Structure Calculations. Density functional theory calculations for $Yb(IO_3)_3$ were carried out using generalized gradient approximation.[22] The Perdew−Burke−Ernzerhof exchange-correlation functional was performed using Vienna ab initio simulation package.[23,24]

Photocatalytic Evaluation. The photocatalytic activities of the $Ln(IO_3)_3$ products were estimated by monitoring the degradation of MO dye and 2,4-DCP in aqueous solution. A 22 W lamp was used to provide UV light. In a typical procedure, 0.1 g of $Ln(IO_3)_3$ was suspended in an MO or 2,4-DCP solution (100 mL, 20 mg/L) under stirring. The mixture was stirred in the darkness for 1 h to achieve the equilibrium of the adsorption/desorption. At set intervals, about 5 mL aliquots from the beaker were taken out for analysis. The photocatalytic efficiencies were characterized by a PERSEE TU-1810 UV−vis spectrophotometer.

RESULTS AND DISCUSSION

As shown in Figure 1a, the diffraction peaks are assigned to monoclinic $Yb(IO_3)_3$ (space group: $P121/n1$; a = 8.6664(9) Å, b = 5.9904(6) Å, c = 14.8862(15) Å, α = 90.00°, β = 96.931(2)°, γ = 90.00°, ICSD: 416690). No other impurities are found, and the peaks are sharp, from which we infer that the as-prepared product has a high purity and crystallinity. The lattice spacing of the monoclinic crystal can be calculated by eq 1:

$$\frac{1}{d^2} = \frac{h^2}{a^2 \sin^2\beta} + \frac{k^2}{b^2} + \frac{l^2}{c^2 \sin^2\beta} - \frac{2hl\cos\beta}{ac \sin^2\beta} \quad (1)$$

where d is the lattice spacing, $\{h, k, l\}$ are the Miller index, and a, b, c, and β are the cell parameters. Therefore, the lattice spacing of crystal facets can be calculated and are marked on the XRD pattern. XRD patterns of other $Ln(IO_3)_3$ products are shown in Figure 1b. We can see that the results show that this series of photocatalysts exhibit almost the same crystal structure. The XRD peaks are indexed to a monoclinic crystal system, and the space group of the crystal structure of all products belongs to $P121/n1$. Thus, we selected $Yb(IO_3)_3$ as a typical case to study the properties of $Ln(IO_3)_3$ products.

SEM images (Supporting Information, Figure S1) show that the as-prepared $Ln(IO_3)_3$ products are composed of particles that display typically aggregated morphologies with large size. HRTEM image (Figure 2) reveals that the particles are

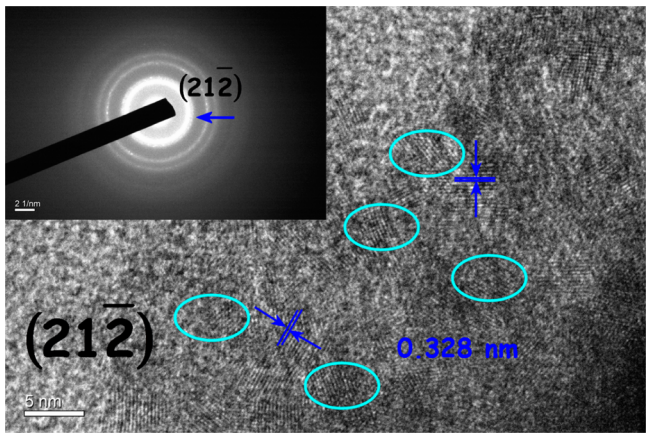

Figure 2. Typical HRTEM image of as-prepared $Yb(IO_3)_3$ sample and its corresponding SAED pattern (inset).

polycrystalline and made up of a lot of small nanocrystals (indicated by blue circles). The lattice spacing of the nanocrystals is 0.328 nm, which matches the spacing of the (21$\bar{2}$) crystal plane of $Yb(IO_3)_3$, in agreement with the XRD results. The corresponding diffraction rings of the SAED pattern (inset in Figure 2) identify the polycrystalline nature of the $Yb(IO_3)_3$ product, and the one conspicuous reflection

dx.doi.org/10.1021/ic500027f | Inorg. Chem. 2014, 53, 4989−4993

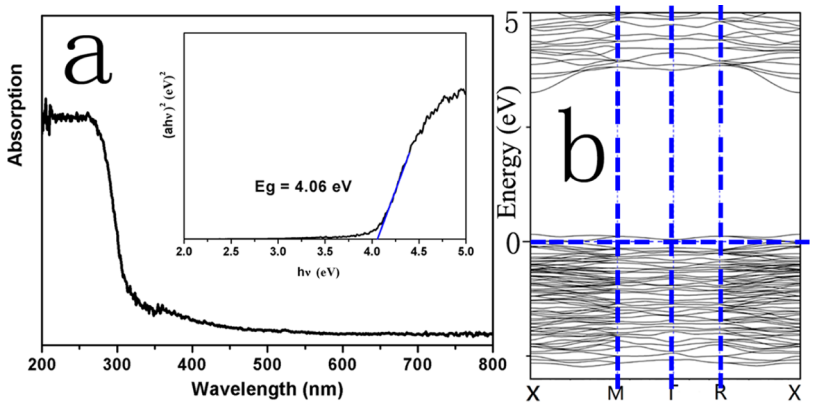

Figure 3. (a) UV–vis DRS spectrum and the associated $(\alpha h\nu)^2$ vs $(h\nu)$ plot (inset) of the $Yb(IO_3)_3$ sample. (b) Calculated electronic band structure of as-prepared $Yb(IO_3)_3$ product. Horizontal blue dash line represents Fermi level.

observed corresponded to a spacing of about 0.328 nm, which is attributed to the $(21\bar{2})$ reflection of $Yb(IO_3)_3$ crystals.

The optical property of the $Yb(IO_3)_3$ product was studied by UV–vis DRS spectroscopy (Figure 3a). Pure $Yb(IO_3)_3$ shows the absorption edge around 300 nm. The band gap can be calculated from the equation $\alpha h\nu = A(h\nu - E_g)^{n/2}$,[25] where α, ν, A, and E_g are absorption coefficient, light frequency, a constant, and band gap, respectively. From Figure 3b, we can see that the maximum of the valence band (VB) and the minimum of the conduction band (CB) lie at the same point. Thus, for $Yb(IO_3)_3$, $n = 1$ for direct transition.[26] From the $(\alpha h\nu)^2$ versus $h\nu$ plot (inset of Figure 3a), the E_g is found to be 4.06 eV based on the x-intercept. The VB potential can be estimated by empirical formulas 2 and 3:[27]

$$E_{VB} = \chi - E^e + 0.5E_g \quad (2)$$

$$E_{CB} = E_{VB} - E_g \quad (3)$$

where E_{VB} is the VB edge potential, χ is the electronegativity of the material, defined as the geometric mean of the absolute electronegativity of the component atoms, E^e is the energy of free electrons on the hydrogen scale (4.5 eV), and E_{CB} is the conduction band edge potential. The χ value of $Yb(IO_3)_3$ is about 6.83 eV, and the E_{VB} and E_{CB} are calculated to be 4.36 and 0.3 eV, respectively.

The different photocatalytic properties are fundamentally caused by two factors, light absorption and quantum efficiency. Figure 4 denotes the UV–vis DRS spectra of the $Ln(IO_3)_3$ products (see details in Supporting Information, Figure S2). We can see in the UV region all products have strong absorption. The absorption spectra of $Nd(IO_3)_3$, $Eu(IO_3)_3$, and $Er(IO_3)_3$ are composed by some sharp peaks at the wavelengths larger than 350 nm, caused by internal transitions.[10] The absorption spectra of $Gd(IO_3)_3$ and $Yb(IO_3)_3$ exhibit clear-cut absorption edges at about 300 nm. Red shift is observed for $Ce(IO_3)_3$. The colors of as-prepared $Ln(IO_3)_3$ samples are yellow, violet, light pink, colorless, pink, and colorless, respectively (Supporting Information, Figure S3), which is consistent with the absorption results. So we selected UV light to study the photocatalytic properties of the products.

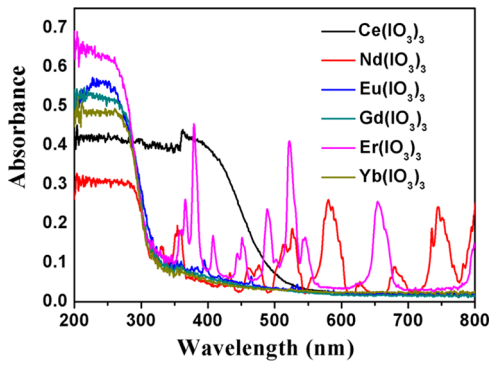

Figure 4. UV–vis DRS spectra of the $Ln(IO_3)_3$ samples.

From Figure 5a, we can see that, in the presence of $Yb(IO_3)_3$, the absorption maximized at 464 nm decreases step by step with illumination time and almost utterly vanishes after 1 h. Figure 5b shows the photocatalytic activities of different photocatalysts. The variation of MO concentration is expressed as C/C_0, where C and C_0 stand for the residual and original concentrations, respectively. For the UV light-active photocatalysts, their activity comparison with that of the benchmark photocatalyst P25 is of significance, so we studied the photocatalytic property of P25 under the same conditions. From Figure 5b, we can see that the photolysis of MO is very low without photocatalysts. In the case of $Ln(IO_3)_3$ (Ln = Ce, Nd, Eu, Gd, Er, Yb) products and P25, about 74%, 50%, 44%, 73%, 62%, 77%, and 45%, respectively, of MO is decomposed after irradiation for 1 h.

Most of the as-prepared $Ln(IO_3)_3$ products have better photocatalytic properties than P25. $Ln(IO_3)_3$ products display typically aggregated morphologies, so their specific surface areas are smaller than P25. So we can obtain higher properties by improving the surface areas of the products. The highest activity is obtained over the $Yb(IO_3)_3$ sample, and the photocatalytic efficiencies of $Ce(IO_3)_3$, $Gd(IO_3)_3$, and $Yb(IO_3)_3$ are similar, which are better than those of $Nd(IO_3)_3$, $Eu(IO_3)_3$, and $Er(IO_3)_3$. Because of their similar structural and electronic properties, the differences of Ln-based iodates may be derived from their essential attributes. With the increase of atomic number of Ln elements, proton number and 4f electrons increase gradually. The shielding effect of 4f electrons to nuclei is weaker than it is to inner electrons, so the effective nuclear charge increases. Thus, nucleic attraction for extranuclear electrons is enhanced, and the ionic radii gradually reduce. The transfer of the electrons that take part in the photocatalytic reaction is suppressed, which is adverse to the photocatalytic efficiency. So as the atomic number increases, the photocatalytic properties of the $Ln(IO_3)_3$ products deteriorate. But Gd^{3+} has a special electronic structure in

dx.doi.org/10.1021/ic500027f | Inorg. Chem. 2014, 53, 4989–4993

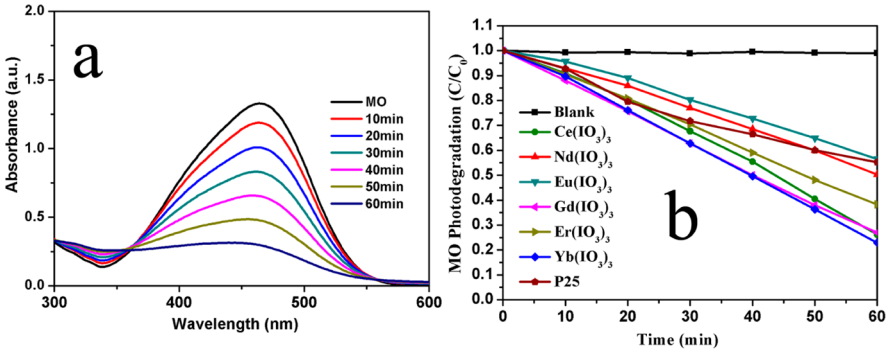

Figure 5. (a) The absorption spectra changes of the MO solution with $Yb(IO_3)_3$ sample under UV light. (b) Photodegradation of MO with time in the presence of different photocatalysts.

which the 4f electrons are in a half-full state, which is stable and makes the 4f electrons have a better shielding effect on the nuclei, so $Gd(IO_3)_3$ has better photocatalytic properties.

In addition to the decoloration of MO, we selected 2,4-DCP, which can not absorb UV−vis light, to further explore the photocatalytic activities of the $Ln(IO_3)_3$ products. In the presence of $Yb(IO_3)_3$, the absorption peak of 2,4-DCP solution at 284 nm decreases with the increase of illumination time (Figure 6), which can prove the MO photodegradation is not

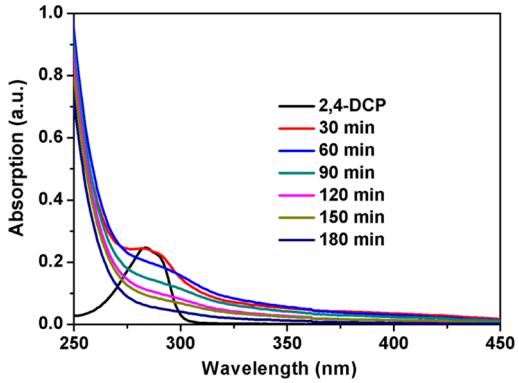

Figure 6. Absorption spectra changes of the 2,4-DCP solution with $Yb(IO_3)_3$ sample under UV light.

caused by the photosensitization process. To evaluate the photostability of the products, the cyclic tests for the photodecomposition of MO were carried out, shown in Supporting Information, Figure S4. The photocatalyst is stable under repeated applications without exhibiting any significant loss of activity.

CONCLUSION

In summary, we have hydrothermally synthesized $Ln(IO_3)_3$ (Ln = Ce, Nd, Eu, Gd, Er, Yb) polycrystals. All the $Ln(IO_3)_3$ products have strong absorption in the UV region. The as-prepared $Ln(IO_3)_3$ products exhibit excellent UV light-driven photocatalytic activities toward the degradation of MO. The maximum efficiency is achieved over the $Yb(IO_3)_3$ sample, and about 77% of MO is decomposed after irradiation for 1 h. The properties of $Ce(IO_3)_3$, $Gd(IO_3)_3$, and $Yb(IO_3)_3$ are similar, which are better than those of $Nd(IO_3)_3$, $Eu(IO_3)_3$, and $Er(IO_3)_3$. The difference may be caused by their essential attributes. As one category of novel promising photocatalysts sensitive to UV light, the Ln-based iodates could be used to alleviate water pollution in future.

ASSOCIATED CONTENT

Supporting Information

Typical SEM images, UV−vis DRS spectra, the colors of the $Ln(IO_3)_3$ samples, and cyclic tests of the photodegradation of MO. This material is available free of charge via the Internet at http://pubs.acs.org.

AUTHOR INFORMATION

Corresponding Author

*E-mail: bbhuang@sdu.edu.cn. Fax: (+86)0531-88365969. Phone: (+86)0531-88365969.

Notes

The authors declare no competing financial interest.

ACKNOWLEDGMENTS

This project was supported by research grants from the National Natural Science Foundation of China (Nos. 21333006, 11374190, and 51021062) and 973 program (No. 2013CB632401).

REFERENCES

(1) Morss, L. R. *Chem. Rev.* **1976**, *76*, 827−841.
(2) Zheng, Y.; Camara, M.; Daiguebonne, C.; Guillou, O.; Bernot, K.; Calvez, G.; Dret, F. L.; Kerbellec, N. *Inorg. Chim. Acta* **2013**, *401*, 11−18.
(3) Eliseeva, S. V.; Bünzli, J.-C. G. *Chem. Soc. Rev.* **2010**, *39*, 189−227.
(4) Bünzli, J.-C. G.; Piguet, C. *Chem. Soc. Rev.* **2005**, *34*, 1048−1077.
(5) de Lill, D. T.; de Bettencourt-Dias, A.; Cahill, C. L. *Inorg. Chem.* **2007**, *46*, 3960−3965.
(6) Serre, C.; Millange, F.; Thouvenot, C.; Gardant, N.; Pellé, F.; Férey, G. *J. Mater. Chem.* **2004**, *14*, 1540−1543.
(7) Kitagawa, H. *Nat. Chem.* **2009**, *1*, 689−690.
(8) Shigematsu, A.; Yamada, T.; Kitagawa, H. *J. Am. Chem. Soc.* **2011**, *133*, 2034−2036.
(9) Zou, Z.; Ye, J.; Arakawa, H. *Top. Catal.* **2003**, *22*, 107−110.
(10) Machida, M.; Murakami, S.; Kijima, T.; Matsushima, S.; Arai, M. *J. Phys. Chem. B* **2001**, *105*, 3289−3294.
(11) Zou, Z.; Ye, J.; Arakawa, H. *J. Phys. Chem. B* **2002**, *106*, 517−520.
(12) Eddaoudi, M.; Kim, J.; Rosi, N.; Vodak, D.; Wachter, J.; O'Keeffe, M.; Yaghi, O. M. *Science* **2002**, *295*, 469−472.
(13) Devic, T.; Serre, C.; Audebrand, N.; Marrot, J.; Férey, G. *J. Am. Chem. Soc.* **2005**, *127*, 12788−12789.
(14) Zou, W.; Visser, C.; Maduro, J. A.; Pshenichnikov, M. S.; Hummelen, J. C. *Nat. Photonics* **2012**, *6*, 560−564.
(15) Fischer, S.; Goldschmidt, J.; Loper, P.; Bauer, G.; Bruggemann, R.; Kramer, K.; Biner, D.; Hermle, M.; Glunz, S. *J. Appl. Phys.* **2010**, *108*, 044912−044912−11.

(16) Haase, M.; Schäfer, H. *Angew. Chem., Int. Ed.* **2011**, *50*, 5808−5829.
(17) Qin, W.; Zhang, D.; Zhao, D.; Wang, L.; Zheng, K. *Chem. Commun.* **2010**, *46*, 2304−2306.
(18) Xu, A.-W.; Gao, Y.; Liu, H.-Q. *J. Catal.* **2002**, *207*, 151−157.
(19) Li, Y.; Song, Z.; Li, C.; Wan, R.; Qiu, J.; Yang, Z.; Yin, Z.; Yang, Y.; Wang, X.; Wang, Q. *Ceram. Int.* **2013**, *39*, 8911−8916.
(20) Li, C.; Wang, F.; Zhu, J.; Yu, J. C. *Appl. Catal., B* **2010**, *100*, 433−439.
(21) Wang, W.; Huang, B.; Ma, X.; Wang, Z.; Qin, X.; Zhang, X.; Dai, Y.; Whangbo, M.-H. *Chem.—Eur. J.* **2013**, *19*, 14777−14780.
(22) Perdew, J. P.; Burke, K.; Ernzerhof, M. *Phys. Rev. Lett.* **1996**, *77*, 3865−3868.
(23) Kresse, G.; Furthmüller, J. *Phys. Rev. B* **1996**, *54*, 11169−11186.
(24) Kresse, G.; Joubert, D. *Phys. Rev. B* **1999**, *59*, 1758−1775.
(25) Cheng, H.; Huang, B.; Dai, Y.; Qin, X.; Zhang, X. *Langmuir* **2010**, *26*, 6618−6624.
(26) Hwang, D. W.; Lee, J. S.; Li, W.; Oh, S. H. *J. Phys. Chem. B* **2003**, *107*, 4963−4970.
(27) Xu, Y.; Schoonen, M. A. *Am. Mineral.* **2000**, *85*, 543−556.

dx.doi.org/10.1021/ic500027f | *Inorg. Chem.* 2014, 53, 4989−4993